JPE 15-3-15

http://dx.doi.org/10.6113/JPE.2015.15.3.721
ISSN(Print): 1598-2092 / ISSN(Online): 2093-4718

Wide-Range Sensorless Control for SPMSM Using an Improved Full-Order Flux Observer

Kyoung-Gu Lee*, June-Seok Lee*, and Kyo-Beum Lee†

*†Department of Electrical and Computer Engineering, Ajou University, Suwon, Korea

Abstract

A sensorless control method was recently investigated in the robot and automation industry. This method can solve problems related to the rise of manufacturing costs and system volume. In a vector control method, the rotor position estimated in the sensorless control method is generally used. This study is based on a conventional full-order flux observer. The proposed full-order flux observer estimates both currents and fluxes. Estimated d- and q-axis currents and fluxes are used to estimate the rotor position. In selecting the gains, the proposed full-order flux observer substitutes gain *k* for the speed information in the denominator of the gain for fast convergence. Therefore, accurate speed control in a low-speed region can be obtained because gains do not influence the estimation of the rotor position. The stability of the proposed full-order flux observer is confirmed through a root-locus method, and the validity of the proposed observer is experimentally verified using a surface permanent-magnet synchronous motor.

Key words: Flux observer, Full-order flux observer, Low-speed sensorless, Sensorless, Surface-permanent magnet synchronous motor

I. INTRODUCTION

Permanent-magnet synchronous motors (PMSMs) have high efficiency because rotor winding is not required to generate magnetic flux. Industries have, therefore, recently begun to use PMSMs, which are operated through a vector control method. The vector control method requires speed information and rotor position for the independent control of torque and flux. Speed information and rotor position can be obtained from sensors, such as an encoder and a resolver. However, sensors have disadvantages because of noise, increased volume of the system, and cost from sensor malfunction [1], [3], [13].

The present study uses full-order flux observer among many sensorless control methods. Full-order flux observer is a method to estimate both currents and fluxes. In a full-order flux observer, errors between estimated currents and real currents are used as inputs, and estimated fluxes are used to calculate the rotor angle. Conventional full-order flux observer has gains to estimate currents and fluxes of d- and q-axis. However, gains to estimate fluxes include speed information in the denominator, which has the disadvantage of increasing gain values in a low-speed region. Hence, the conventional full-order flux observer includes a ripple because of the increased gain values, which generate a speed error value at low speed [1]-[12].

Therefore, in this study, the proposed full-order flux observer removes speed information from the denominator of the gain to estimate fluxes, and gain *k* for fast convergence characteristic is added instead. Gain *k* without speed information in the denominator does not influence a low-speed region. The estimated fluxes of the d- and q-axis are used to estimate the rotor angle, and the estimated speed obtained from the rotor angle does not have a speed error value in the low-speed region.

The estimated speed is calculated through the speed estimation method through a proportional-integral (PI) controller. A PI controller generally has a simple structure and is commonly used because of its short calculation time. The input of a PI controller uses the error value of the feedback rotor angle, which is changed from the integral value by the estimated speed. Therefore, the speed error value of the PI speed controller converges to values near zero. The

Manuscript received Oct. 8, 2014; accepted Jan. 22, 2015
Recommended for publication by Associate Editor Gaolin Wang.
†Corresponding Author: kyl@ajou.ac.kr
Tel: +82-31-219-2376, Fax: +81-31-9531, Ajou University
*Department of Electrical and Computer Engineering, Ajou University, Korea

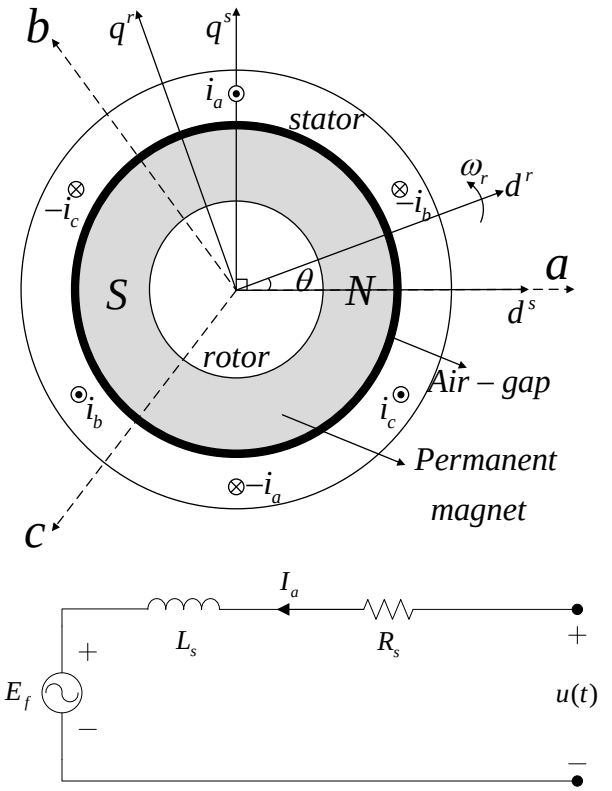

Fig. 1. Interior structure and equivalent circuit of the SPMSM.

output, which is an angular speed, is the sum of the values generated through proportion and integration [10].

In the current study, the stability of the proposed full-order flux observer with the improved gain is verified through a root-locus method. The simulation of the root-locus method is performed using a MATLAB tool. Furthermore, the estimation performance of the proposed algorithm over a wide range is experimentally confirmed.

II. Flux Modeling of SPMSM

The stator winding of a surface permanent-magnet synchronous motor (SPMSM) generates a rotating magnetic field. The rotor rotates synchronously with the magnetic field. The rotor of an SPMSM is also a permanent cylindrical magnet. Therefore, the effective air gap of SPMSM is constant, and the inductance values of the d- and q-axis are equal. The d-axis of the stationary coordinate system is in the pole direction of the permanent magnet, and the q-axis forms a right angle to the d-axis. The d- and q-axis of the synchronous coordinate system rotate along with the rotating magnetic field. Fig. 1 shows the structure and equivalent circuit of SPMSM [1]-[3].

III. Full-Order Flux Observer

The d- and q-axis flux values of the full-order flux observer are directly affected by current [1]-[3]. Therefore, detected current values are only used in error information; estimated currents are used directly to estimate the d- and q-axis fluxes.

However, the full-order flux observer is only used for the detected currents to obtain error information; the observer uses estimated currents to estimate the d- and q-axis fluxes. Therefore, the full-order flux observer does not generate distortion by estimating currents and fluxes. It also has advantages in terms of load change and disturbances when estimating currents and fluxes [1]-[6].

A. Full-Order Flux Observer

The voltage equation of the stationary coordinate system of SPMSM is expressed as

$$\begin{bmatrix} v_{ds} \\ v_{qs} \end{bmatrix} = \begin{bmatrix} R_s & 0 \\ 0 & R_s \end{bmatrix} \begin{bmatrix} i_{ds} \\ i_{qs} \end{bmatrix} + \begin{bmatrix} -\lambda_{qs} \\ \lambda_{ds} \end{bmatrix}. \quad (1)$$

The d- and q-axis fluxes, namely, λ_{ds} and λ_{qs} respectively, are defined as

$$\lambda = \begin{bmatrix} \lambda_{ds} \\ \lambda_{qs} \end{bmatrix} = p \begin{bmatrix} L_s & 0 \\ 0 & L_s \end{bmatrix} \begin{bmatrix} i_{ds} \\ i_{qs} \end{bmatrix} + \omega_{re} \lambda_f \begin{bmatrix} \cos\theta \\ \sin\theta \end{bmatrix}, \quad (2)$$

where λ_f is the permanent magnet flux, and the current and voltage use values of the synchronous reference frame [1]–[3].

Hence, Eq. (3) shows the d- and q-axis matrix structures of the full-order flux observer from Eqs. (1) and (2):

$$p\hat{x} = \begin{bmatrix} -\frac{R_s}{L_s} & 0 & 0 & -\frac{\hat{\omega}_{re}}{L_s} \\ 0 & -\frac{R_s}{L_s} & \frac{\hat{\omega}_{re}}{L_s} & 0 \\ 0 & 0 & 0 & -\hat{\omega}_{re} \\ 0 & 0 & \hat{\omega}_{re} & 0 \end{bmatrix} \begin{bmatrix} \hat{i}_{ds} \\ \hat{i}_{qs} \\ \hat{\lambda}_{ds} \\ \hat{\lambda}_{qs} \end{bmatrix} + \begin{bmatrix} \frac{1}{L_s} & 0 \\ 0 & \frac{1}{L_s} \\ 0 & 0 \\ 0 & 0 \end{bmatrix} \begin{bmatrix} v_{ds} \\ v_{qs} \end{bmatrix} + \begin{bmatrix} h_{11} & 0 \\ 0 & h_{11} \\ h_{21} & 0 \\ 0 & h_{21} \end{bmatrix} + \begin{bmatrix} 0 & -h_{21} \\ h_{21} & 0 \\ 0 & -h_{22} \\ h_{22} & 0 \end{bmatrix} (\hat{i} - i), \quad (3)$$

where h_{11}, h_{12}, h_{21}, and h_{22} are the gains of the full-order flux observer.

From the d- and q-axis fluxes, the information on the rotor angle is expressed as

$$\hat{\theta} = \arctan\left(\frac{\hat{\lambda}_{ds}}{\hat{\lambda}_{qs}} \right). \quad (4)$$

B. Conventional Gain of the Full-Order Flux Observer

The gain of the full-order flux observer is determined from the flux modeling of SPMSM. Hence, the system characteristic equation is defined as

$$\left|sI - A - Hc\right| = (s + \frac{R_s}{L_s} - h_{11} - jh_{12})(s - j\hat{\omega}_{re}) + \frac{j\hat{\omega}_{re}}{L_s}(h_{21} + jh_{22}) \quad . \quad (5)$$

The roots of the second-order equation are determined by $\alpha_1+j\beta_1$ and $\alpha_2+j\beta_2$, and are expressed as

$$(s-(\alpha_1 + j\beta_1))(s-(\alpha_2 + j\beta_2)) = s^2 - (\alpha_1 + j\beta_1 + \alpha_2 + j\beta_2)s + (\alpha_1 + j\beta_1)(\alpha_2 + j\beta_2) \quad . \quad (6)$$

The second-order equation, which is Eq. (6), can be defined by dividing the real and imaginary numbers from Eqs. (7) and (8) [1]-[6], [8], [9]. Equation (7) is used to obtain the gain of the current, while Eq. (8) is used to obtain the gain of the flux:

$$h_{11} + jh_{12} = \frac{R_s}{L_s} - j\hat{\omega}_{re} + \alpha_1 + j\beta_1 + \alpha_2 + j\beta_2 \,, \quad (7)$$

$$h_{21} + jh_{22} = -(\alpha_1 + \alpha_2)L_s + j\hat{\omega}_{re} \cdot L_s - j\frac{L_s}{\hat{\omega}_{re}}(\alpha_1 + j\beta_1)(\alpha_2 + j\beta_2) \,, \quad (8)$$

$$\beta_1 = \beta_2 = 0 \,. \quad (9)$$

Coefficients $\beta 1$ and $\beta 2$ are defined as 0 from Eq. (9) for a stable pole placement [1]–[3]. Hence, h_{11}, h_{12}, h_{21}, and h_{22} are defined as

$$h_{11} = \frac{R_s}{L_s} + \alpha_1 + \alpha_2 \,, \quad (10)$$

$$h_{12} = -j\hat{\omega}_{re} \,, \quad (11)$$

$$h_{21} = -(\alpha_1 + \alpha_2)L_s \,, \quad (12)$$

$$h_{22} = j\hat{\omega}_{re}L_s - \left(j\frac{L_s(\alpha_1\alpha_2)}{\hat{\omega}_{re}}\right). \quad (13)$$

Thus, Eq. (13) includes the speed information from the denominator.

When the speed information is included in the denominator, the gain increases because of the low value of the speed and becomes an important factor in the deterioration of estimation performance [1]-[3]. Consequently, at low speed, the estimated currents and fluxes containing ripples decrease the estimation performance. The estimated rotor angle is the distorted swing to the decrease in estimation performance. Hence, the rotor cannot perform precise speed control at low speed.

C. *Proposed Gain of the Full-Order Flux Observer*

To solve the problem at low speed in a conventional full-order flux observer, the speed information of the denominator is eliminated and gain k is added for fast offset convergence. The proposed gain is not affected by the estimation performance at low speed. Precise sensorless speed control becomes feasible by obtaining accurate position information on the rotor from the estimated flux, which does not contain ripples. The gain variables h_{11}, h_{12}, h_{21}, and h_{22} of the full-order flux observer are defined as

$$h_{11} = \frac{R_s}{L_s} + \alpha_1 + \alpha_2 \,, \quad (14)$$

$$h_{12} = -j\hat{\omega}_{re} \,, \quad (15)$$

$$h_{21} = -(\alpha_1 + \alpha_2)L_s \,, \quad (16)$$

$$h_{22} = j\hat{\omega}_{re}L_s - k\left(jL_s(\alpha_1\alpha_2)\right), \quad (17)$$

respectively, where the coefficients β_1 and β_2 are 0 for stable pole placement. Equation (17) eliminates the speed information in the denominator [1], [3], [8], [9].

Hence, the gain value does not increase owing to the absence of the speed information when gain k is added for fast offset convergence and stable pole placement.

D. *Stability of the Proposed Observer*

Equation (18) is used to obtain the gain of the estimated current, while Eq. (19) is used to obtain the gain of the estimated flux.

$$h_{11} + jh_{12} = \frac{R_s}{L_s} - j\hat{\omega}_{re} + \alpha_1 + \alpha_2 \,, \quad (18)$$

$$h_{21} + jh_{22} = -(\alpha_1 + \alpha_2)L_s + j\hat{\omega}_{re}L_s - k(jL_s(\alpha_1\alpha_2)) \,, \quad (19)$$

where h_{11} and h_{21} are the real parts, and h_{21} and h_{22} are the imaginary parts. Furthermore, α_1 and α_2 are the values of −75 and −1,400.

$$\dot{x} = A_x + B_x$$
$$y = C_x$$
$$A = \begin{bmatrix} -\frac{R_s}{L_s} + h_{11} + jh_{12} & -\frac{j\hat{\omega}_{re}}{L_s} \\ h_{21} + jh_{22} & j\hat{\omega}_{re} \end{bmatrix}. \quad (20)$$
$$B = \begin{bmatrix} -j\frac{1}{L_s} \\ j \end{bmatrix}$$

In accordance with Eq. (20), the state-space equation is redefined as

$$G_{(s)} = C\left[sI - A\right]^{-1}B$$
$$C = \begin{bmatrix} 0 & 1 \end{bmatrix}, \quad I = \begin{bmatrix} 0 & 1 \\ 1 & 0 \end{bmatrix}. \quad (21)$$

$[sI\text{-}A]^{-1}$ is defined as

$$\left[sI - A\right]^{-1} = \begin{bmatrix} \frac{d}{ad-bc} & -\frac{b}{ad-bc} \\ -\frac{c}{ad-bc} & \frac{a}{ad-bc} \end{bmatrix}$$
$$a = s - \alpha_1 - \alpha_2 + j\hat{\omega}_{re}$$
$$c = (\alpha_1 + \alpha_2)L_s - j\hat{\omega}_{re}L_s + jkL_s(\alpha_1\alpha_2) \quad . \quad (22)$$
$$b = \frac{j\hat{\omega}_{re}}{L_s}$$
$$d = s - j\hat{\omega}_{re}$$
$$ad - bc = s^2 - s(\alpha_1 + \alpha_2) - k\hat{\omega}_{re}(\alpha_1\alpha_2)$$

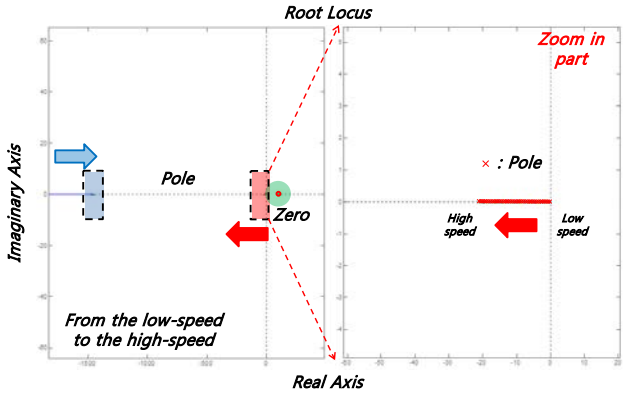

(a) k = 0.001.

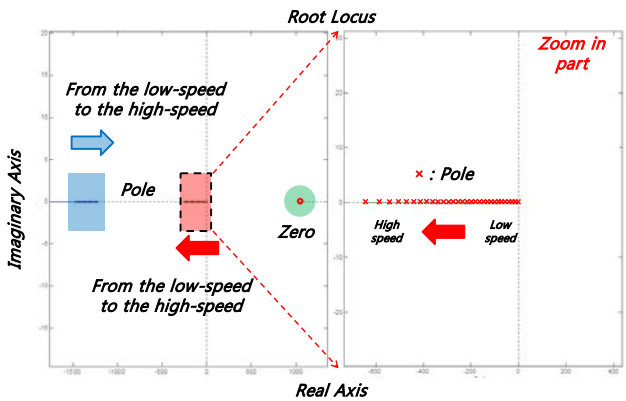

(b) k = 0.01.

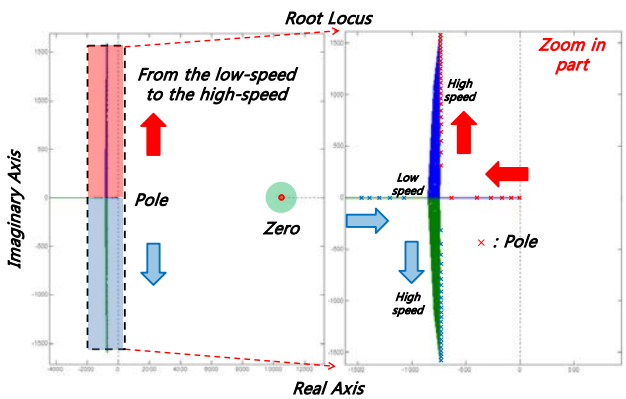

(c) k = 0.1.

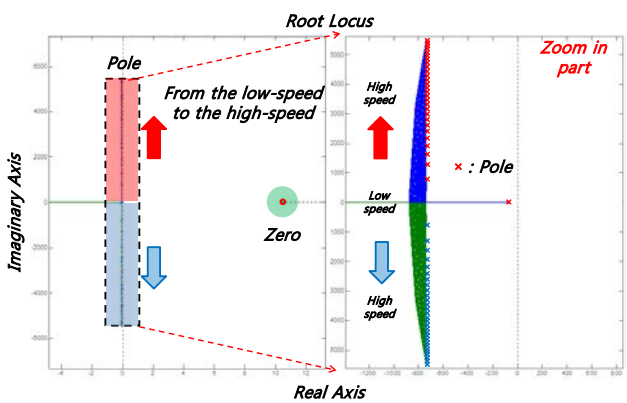

(d) k = 1.

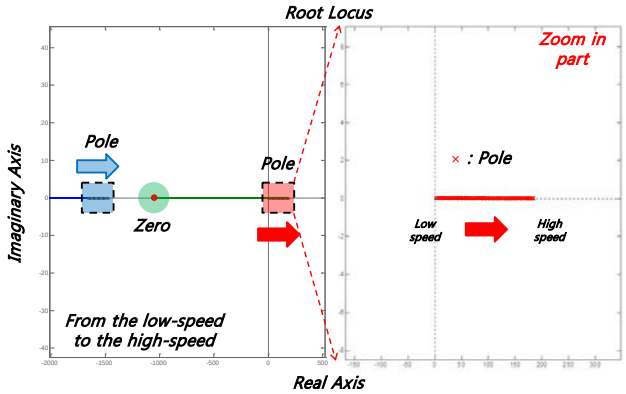

(e) k = −0.01.

Fig. 2. Root-locus stability criterion method by changed gain k.: 10–300 rpm.

Hence, the characteristic equation using Eq. (22) is defined as

$$G_{(s)} = \frac{js - k(\alpha_1\alpha_2)}{s^2 - s(\alpha_1 + \alpha_2) - \hat{\omega}_{re} k(\alpha_1\alpha_2)}. \quad (23)$$

Gains are added k for quick error convergence of the speed. Fig. 2 shows the pole placement depending on the value of k. The stability of the pole placement can be checked according to the pole direction. If the pole is positive, the system is unstable, whereas the system is stable if the pole is negative. A smaller negative value of the pole means a more stable system [1]-[3], [8], [9].

The result in Fig. 2(a) shows the pole placement when k = 0.001. In Fig. 2(a), the pole placement is composed narrowly by the speed change. The area of the narrowly composed pole placement means an almost unstable system in the low-speed range. The result in Fig. 2(b) shows the pole placement when k = 0.01. In Fig. 2(b), the pole placement is composed widely by speed change. The area of the widely composed pole placement means a stable system in the low-speed and high-speed ranges. The result in Fig. 2(c) shows the pole placement when k = 0.1. The pole placement is composed near the value of 0 by the speed change from Fig. 2(c). The narrowly composed pole placement area means an almost unstable system. The result in Fig. 2(d) shows the pole placement when k = 1. From Fig. 2(d), the pole placement is composed narrowly by the speed change. Similarly, the narrowly composed pole placement area means an almost unstable system. The result in Fig. 2(e) shows the pole placement when k = −0.01. The pole placement is an unstable system because of the positive value. An appropriate value of gain k should be used depending on the system. Hence, a value of 0.01 is used for the proposed gain k.

E. Speed Estimation

In general, a PI controller is used for speed estimation [1]-[3], [10]. A PI controller has a simple structure and can control speed through the control gain.

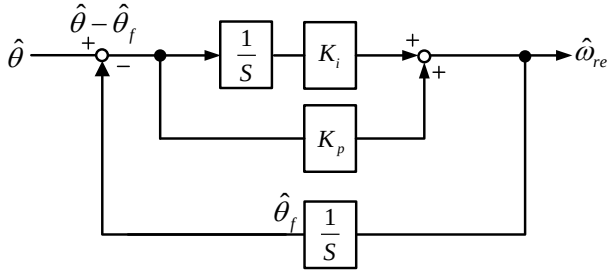

Fig. 3. Block diagram of the PI controller.

TABLE I
VALUES OF THE PROPOSED GAIN

α_1	−75
α_2	−1400
k	0.01
f_{sw}	10 kHz

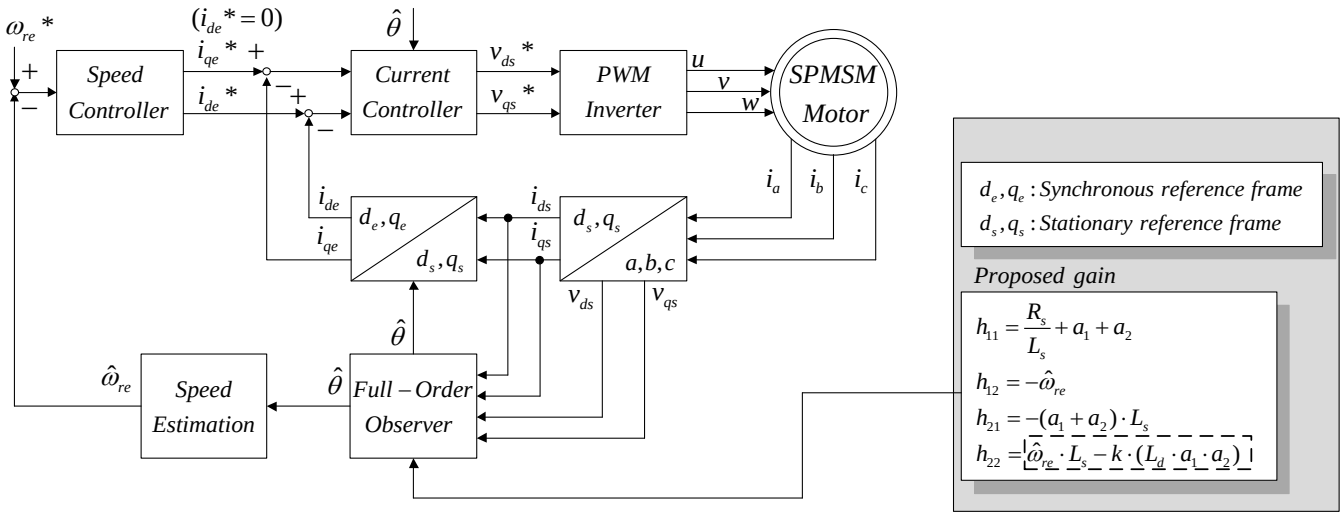

Fig. 4. Overall block diagram of the proposed full-order flux observer.

TABLE II
PARAMETERS OF THE SPMSM

R_s	2.2 Ω
L_s	3.05 mH
P(Pole)	24
λ_f	0.477 Wb
Rated power	3 kW
Rated speed	300 rpm
Peak current	8 A

A PI controller uses the estimated rotor angle to calculate the estimated angular speed. As the estimated angular speed is integrated into the rotor angle through the integral term, the error value between the estimated rotor angle and the integrated rotor angle is used as an input. Fig. 3 shows the block diagram of the PI controller, and Fig. 4 shows the overall block diagram of the proposed full-order flux observer.

In Fig. 3, the P term generates the estimated speed, which is proportional to the error value of the rotor angle, and the P gain determines the response rise and delay times. The I term generates the estimated speed proportional to the accumulated error value, and the I gain reduces the steady-state error. However, because the high control gain of the PI controller vibrates according to the speed, selecting the control gain value is difficult, and the ripple of the estimated speed can increase. If P and I are selected appropriately, the error of the rotor angle will converge to zero, and the output will be the estimated speed [1]-[3], [10]. The rotor angle is estimated by the estimated fluxes of the d- and q-axis via the proposed full-order flux observer. Hence, accurate speed control is required for the accurate d- and q-axis estimated fluxes.

IV. EXPERIMENTAL RESULTS

Table I shows the gains α_1, α_2, and k proposed in this study, while Table II shows the SPMSM parameters used in the experiment. The control period was 100 μs, the switching frequency was 10 kHz, and the dc-link voltage was 550 V. The experiment in this study was performed using the SPMSM parameters in Tables I and II.

Fig. 6 shows the actual rotor angle, estimated rotor angle and estimated d- and q-axis fluxes at 10 rpm. From the experimental results shown in Fig. 6, an improved performance is confirmed. Fig. 7 is the estimated performance of the proposed full-order flux observer. The conventional full-order flux observer, which generates distortion in the rotor angle, included ripples in the estimated

(a)

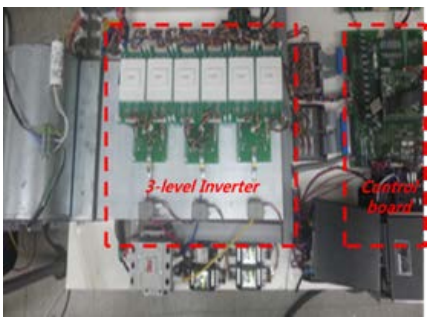

(b)

Fig. 5. Experimental setup. (a) SPMSM. (b) Control board and three-level inverter.

values because the estimated d- and q-axis fluxes were formed by h_{11} and h_{22}. The conventional gain of the full-order flux observer described in Section III included the angular speed in the denominator of the gain. Therefore, the gain at low speed could be greatly increased, which generated distortion in the estimated rotor angle.

The experimental conditions of Fig. 7 were equivalent to those of Fig. 6. The proposed gain did not include speed information. Therefore, the system estimated the d- and q-axis fluxes accurately. The estimated rotor angle also reflected the performance of the rotor angle estimation without the distortion by the d- and q-axis fluxes.

Fig. 8 shows the actual rotor angle, estimated rotor angle, and estimated speed at 10 rpm, illustrating the estimated performances of the conventional full-order flux observer and the proposed full-order flux observer. The estimated speed of the conventional full-order flux observer included ripples from the gain. Furthermore, the estimated speed of the proposed full-order flux observer did not include the ripples from the gain because speed information was not included in the denominator.

Fig. 9 shows the actual rotor angle, estimated rotor angle, actual speed, and A-phase current at 10 rpm under a full-load condition. The current was increased by increasing the load and creating the d- and q-axis fluxes. Therefore, the fluxes could be estimated more accurately by the large currents, and the proposed full-order flux observer shows accurate estimated performance with a full load.

Figs. 10 and 11 show the characteristics when the speed of

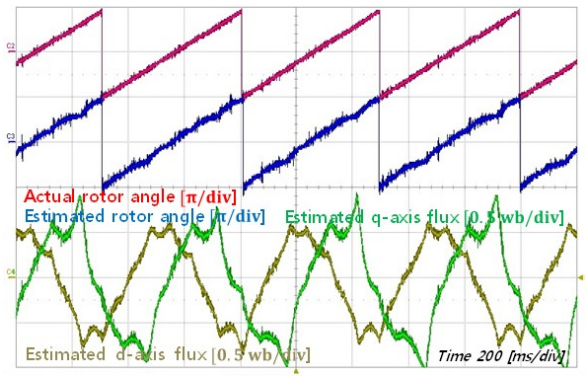

Fig. 6. Conventional full-order flux observer: 10 rpm.

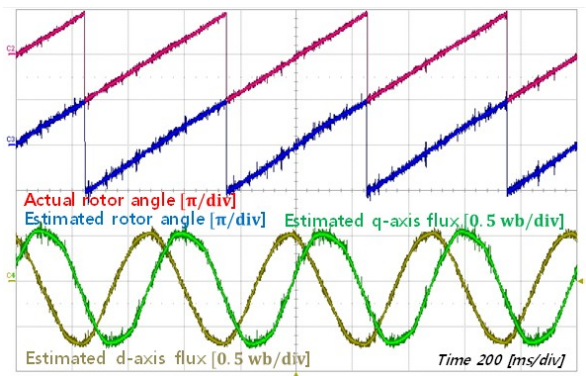

Fig. 7. Proposed full-order flux observer: 10 rpm.

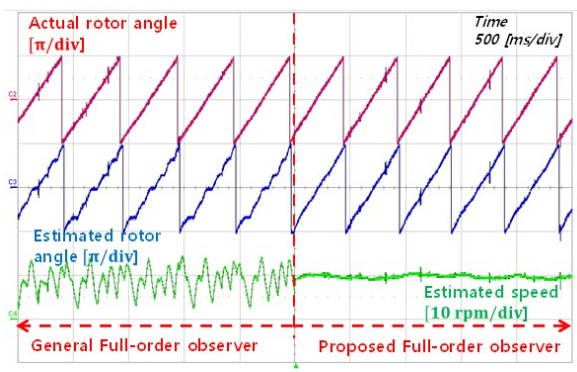

Fig. 8. Performance comparison of full-order flux observers.

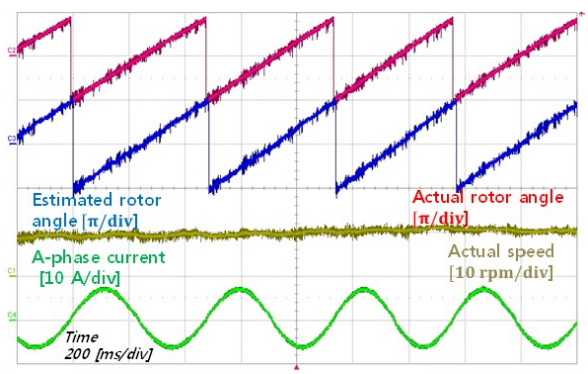

Fig. 9. Proposed full-order flux observer at 10 rpm with full load.

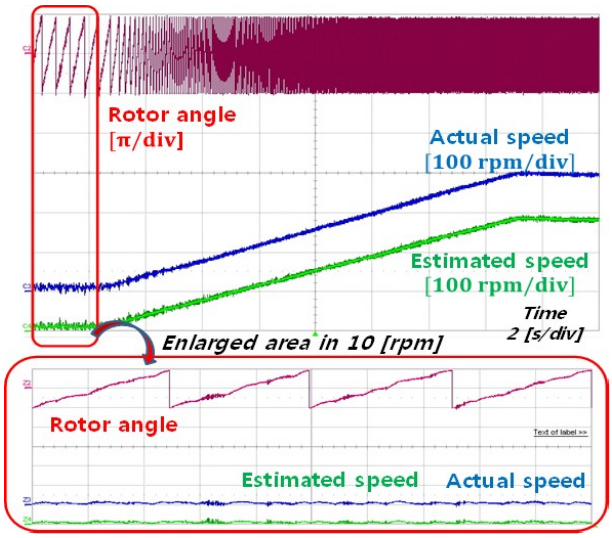

Fig. 10. Speed variable of the conventional full-order flux observer: 10–300 rpm.

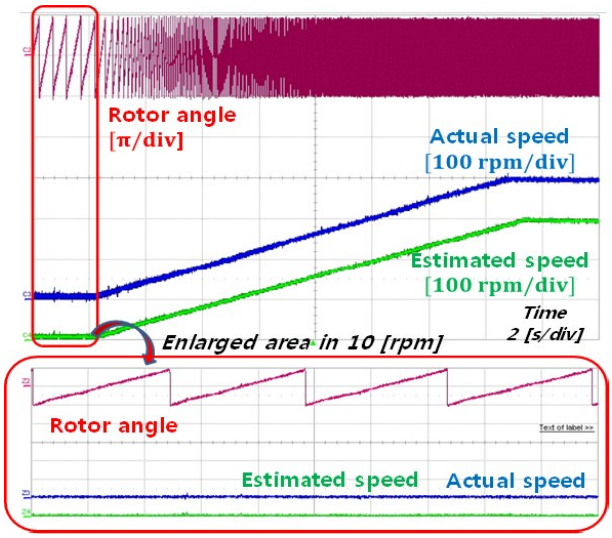

Fig. 12. Speed variable of the proposed full-order flux observer: 10–300 rpm.

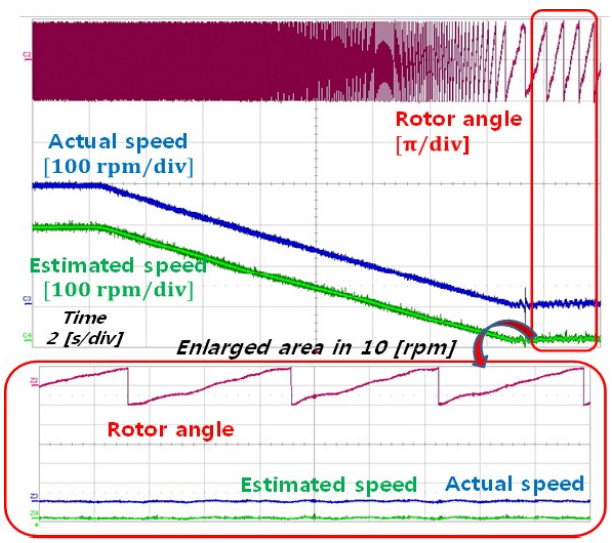

Fig. 11. Speed variable of the conventional full-order flux observer: 300–10 rpm.

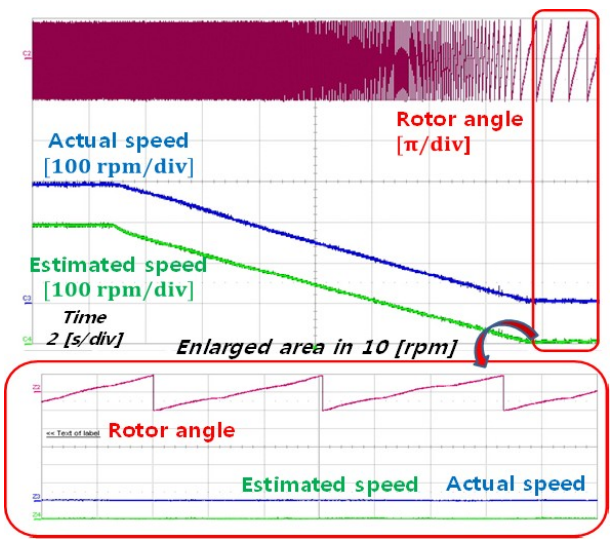

Fig. 13. Speed variable of the proposed full-order flux observer: 300–10 rpm.

the conventional full-order flux observer is changed. The speed changed from 10 rpm to 300 rpm. Fig. 11 shows the change in speed from 300 rpm to 10 rpm. Figs. 10 and 11 show the actual rotor angle, speed, and estimated speed. The enlarged waveforms in the low-speed range are shown at the bottom of Figs. 10 and 11.

The bottom part of Fig. 10 shows an enlarged waveform of 10 rpm. The estimated performance of the conventional full-order flux observer includes a ripple of changed speed.

The bottom part of Fig. 11 is similar to that of Fig. 10, and Fig. 11 shows an enlarged waveform of 10 rpm in the changed speed range from 300 rpm to 10 rpm. The conventional full-order flux observer showed the estimated performance over a wide range of speed regions, but a ripple was included in the low-speed range.

Figs. 12 and 13 also show the characteristics when the speed of the proposed full-order flux observer is changed. The speed changed from 10 rpm to 300 rpm in Fig. 12, whereas the speed changed from 300 rpm to 10 rpm in Fig. 13. Figs. 12 and 13 show the actual rotor angle, speed, and estimated speed. The enlarged waveforms in the low-speed range are shown at the bottom of Figs. 12 and 13.

The bottom part of Fig. 12 shows an enlarged waveform at 10 rpm. The proposed full-order flux observer indicated a stable estimated performance with changed speed.

In addition, the waveform of the estimated performance in the low-speed region did not include a ripple. The bottom part of Fig. 13 is similar to Fig. 12, which shows an enlarged waveform of 10 rpm in the changed speed range from 300 rpm to 10 rpm. The proposed full-order flux observer showed a stable estimated performance over a wide range of speed regions.

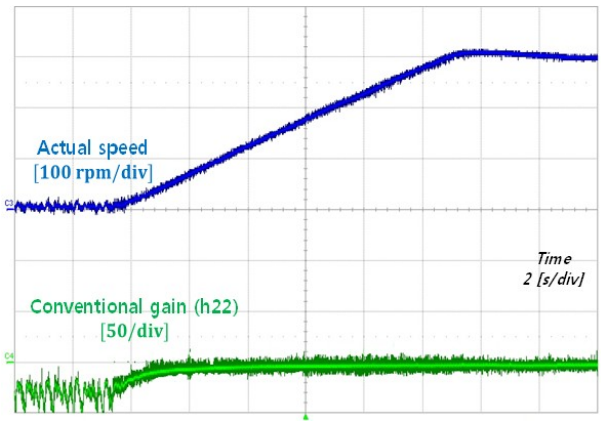

Fig. 14. Dependence of conventional gain on speed.

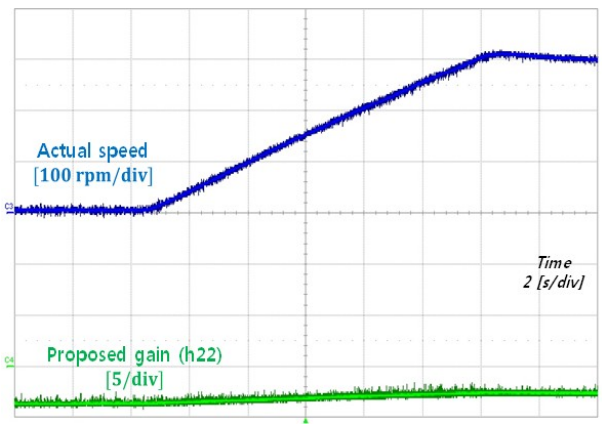

Fig. 15. Dependence of proposed gain on speed.

The full-order flux observer experienced a gain from the changed speed. Therefore, the gain from the changed speed indicated a changed value in Figs. 14 and 15.

Fig. 14 shows the changed value using the conventional gain. The experiment results of the conventional gain showed a ripple in the low-speed region because the denominator of the conventional gain included speed information.

Fig. 15 shows the changed value using the proposed gain. The experiment results of the proposed gain showed stable estimated speed in the low-speed region. Furthermore, the experimental results of the proposed gain did not include a ripple because of the changed speed. Hence, the proposed gain was able to estimate over a wide range of low and high speeds.

V. Conclusion

The conventional full-order flux observer includes speed information in the gain denominator. Hence, the estimated performance is reduced in the low-speed region. However, the proposed full-order flux observer can achieve stable estimation performance for the d- and q-axis fluxes in the low-speed range. Therefore, the proposed full-order flux observer uses accurate estimated flux values that estimate the exact rotor angle. In this study, gain k was added for fast convergence of the error value, and the speed information of the gain denominator was removed. In addition, stable performance of the proposed gain was verified by comparing the proposed and conventional gains.

Therefore, the performance of the accurate speed control of the proposed full-order flux observer was experimentally confirmed.

Acknowledgment

This work was supported by 20134030200310 of the Korea Institute of Energy Technology Evaluation and Planning (KETEP) grant funded by the Korea government Ministry of Knowledge Economy.

This research was also supported by the Basic Science Research Program through the National Research Foundation of Korea (NRF) funded by the Ministry of Education (2013R1A1A2A10006090).

References

[1] H. W. Sim, J. S. Lee, and K. B. Lee, "A simple strategy for sensorless speed control for an IPMSM during startup and over wide speed range," *Journal of Electrical Engineering & Technology*, Vol. 9, No. 5, pp. 1582-1591, Sep. 2014.

[2] A. Matsumoto, M. Hasegawa, M. Tomita, and K. Matsui, "Algebraic design of full-order flux observer for IPMSM position sensorless control," in *Proc. IEEE IEMDC.*, pp. 1276-1281, 2011.

[3] K. G. Lee, J. S. Lee, and K. B. Lee, "SPMSM sensorless control for wide speed range using full-order flux observer," in *Proc. IEEE ICIT.*, pp. 164-168, 2014.

[4] N. K. Quang, N. T. Hieu, and Q. P. Ha, "FPGA-based sensorless PMSM speed control using reduced-order extended Kalman filters," *IEEE Trans. Ind. Electron.*, Vol. 61, No. 12, pp. 6574-6582, Dec. 2014.

[5] Z. Zhifeng, T. R Enyuyan, B. Boadong, and X. Dexin, "Novel direct torque control based on space vector modulation with adaptive stator flux observer for induction motors," *IEEE Trans. Magn.*, Vol. 48, No. 8, pp. 3133-3136, Aug. 2010.

[6] Z. Qu, M. Hinkkanen, and L. Harnefors, "Gain scheduling of a full-order observer for sensorless induction motor drives," *IEEE Trans. Ind. Appl.*, Vol. 50, No. 6, pp. 3834-3845, Nov/Dec. 2014.

[7] M. Hasegawa and K. Matsui, "Position sensorless control for interior permanent magnet synchronous motor using adaptive flux observer with inductance identification," *IET Elect. Power Appl.*, Vol. 3, No. 3, pp. 209-217, May 2009.

[8] S. Po-ngam and S. Sangwongwanich, "Stability and dynamic performance improvement of adaptive full-order observers for sensorless PMSM drive," *IEEE Trans. Power Electron.*, Vol. 27, No. 2, pp. 588–600, Feb. 2012.

[9] X. Ji, F. Wang, and D. Zhang, "Robustness analysis of pole placement method with single degree of freedom in full order flux observer," in *Proc. IEEE APPEEC.*, pp. 1-4, 2012.

[10] L. Harnefors, S. E. Saarakkala, and M. Hinkkanen, "Speed control of electrixcal drives using classical control methods,"

IEEE Trans. Ind. Appl., Vol. 49, No. 2, pp. 889-898, Mar/Apr. 2013.
[11] J. S. Kim, "Development of the zero-phase-error speed controller for high performance PMSM drives," *Transactions of Korean Institute of Power Electronics (KIPE)*, Vol. 19, No. 2, pp. 184-193, Apr. 2014.
[12] H. S. Park and Y. I. Lee, "Torque tracking and ripple reduction of permanent magnet synchronous motor using finite control set-model predictive control (FCS-MPC)," *Transactions of Korean Institute of Power Electronics (KIPE)*, Vol. 19, No. 3, pp. 249-256, Jun. 2014.
[13] S. H. Kim, "Maximum torque operating strategy based on stator flux analysis for direct torque and flux control of a SPMSM," *Transactions of Korean Institute of Power Electronics (KIPE)*, Vol. 19, No. 5, pp. 463-469, Oct. 2014.

Kyoung-Gu Lee received his B.S. degree in Mechatronic Engineering from Korea Polytechnic University, Si-heung, Korea, in 2012. He is currently working toward his M.S. degree at Ajou University, Suwon, Korea. His research interests include electric machine drives and switched reluctance motor drives.

June-Seok Lee received his B.S. and M.S. degrees in Electrical and Computer Engineering from Ajou University, Korea, in 2011 and 2013, respectively. He is currently working toward his Ph.D. degree at Ajou University, Korea. His research interests include grid-connected systems, multilevel inverter, and reliability.

Kyo-Beum Lee received his B.S. and M.S. degrees in Electrical and Electronic Engineering from Ajou University, Korea, in 1997 and 1999, respectively. He received his Ph.D. degree in Electrical Engineering from Korea University, Korea, in 2003. From 2003 to 2006, he worked at the Institute of Energy Technology, Aalborg University, Aalborg, Denmark. From 2006 to 2007, he was with the Division of Electronics and Information Engineering, Chonbuk National University, Jeonju, Korea. In 2007, he joined the School of Electrical and Computer Engineering, Ajou University, Suwon, Korea. He is an associated editor of the Institute of Electrical and Electronics Engineers Transactions on Power Electronics and Journal of Power Electronics. His research interests include electric machine drives, renewable power generations, and electric vehicles.